NJC

Accepted Manuscript

This is an *Accepted Manuscript*, which has been through the Royal Society of Chemistry peer review process and has been accepted for publication.

Accepted Manuscripts are published online shortly after acceptance, before technical editing, formatting and proof reading. Using this free service, authors can make their results available to the community, in citable form, before we publish the edited article. We will replace this *Accepted Manuscript* with the edited and formatted *Advance Article* as soon as it is available.

You can find more information about *Accepted Manuscripts* in the Information for Authors.

Please note that technical editing may introduce minor changes to the text and/or graphics, which may alter content. The journal's standard Terms & Conditions and the Ethical guidelines still apply. In no event shall the Royal Society of Chemistry be held responsible for any errors or omissions in this *Accepted Manuscript* or any consequences arising from the use of any information it contains.

ROYAL SOCIETY OF CHEMISTRY

www.rsc.org/njc

Graphical Abstract:

A new Ru(II) complex $[Ru(phen)_2(addppn)]^{2+}$ was synthesized and characterized. The in vitro cytotoxicity, apoptosis, cellular uptake, cell cycle arrest, ROS and mitochondrial membrane potential, and western blot analysis were investigated. The DNA-binding behaviors were also studied.

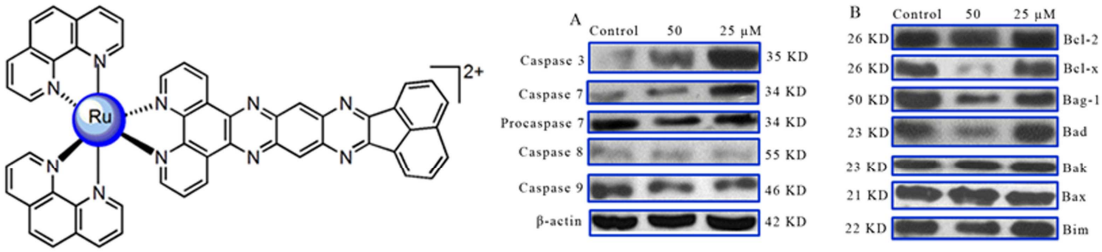

Submitted to New J Chem

Induction of Apoptosis in BEL-7402 Cells through the ROS-mediated Mitochondrial Pathway by Ruthenium(II) Polypyridyl Complex

Guang-Bin Jiang[a], Jun-Hua Yao[b], Ji Wang[a], Wei Li[a], Bing-Jie Han[a], Yang-Yin Xie[a], Gan-Jian Lin[a], Hong-Liang Huang[c,*], Yun-Jun Liu[a,*]

[a]*School of Pharmacy, Guangdong Pharmaceutical University, Guangzhou, 510006, PR China*

[b]*Instrumentation Analysis and Research Center, Sun Yat-Sen University, Guangzhou, 510275, PR China*

[c]*School of Life Science and Biopharmaceutical, Guangdong Pharmaceutical University, Guangzhou, 510006, PR China*

* Corresponding author. Tel: +86 20 39352122; fax: +86 20 39352129.

E-mail address: hhongliang@163.com (H.L. Huang), lyjche@163.com(Y.J. Liu).

Abstract A new Ru(II) polypyridyl complex $[Ru(phen)_2(addppn)](ClO_4)_2$ (Ru1) has been synthesized and characterized. The DNA-binding constant of the complex with DNA was determined to be 1.93 (± 0.12) × 10^6 M^{-1}. The complex interacts with DNA by intercalative mode. Cytotoxicity in vitro, apoptosis, cell cycle distribution, apoptotic pathway, reactive oxygen species and mitochondrial membrane potential assays were performed. The IC_{50} values of Ru1 toward BEL-7402, HeLa, MG-63 and SKBR-3 cell lines are 3.9 ± 0.4, 9.0 ± 0.8, 6.6 ± 0.6 and 5.1 ± 0.6 μM, respectively. Interestingly, Ru1 shows higher cytotoxicity than cisplatin on BEL-7402 cells under identical conditions. Ru1 can effectively induce apoptosis in BEL-7402 and induces cell cycle arrest at the G0/G1 phase on BEL-7402 cells and G2/M phase on SKBR-3 cells. In addition, Ru1 can enhance the level of reactive oxygen species and induce the decrease of mitochondrial membrane potential. Western blot analysis shows that Ru1 activates caspase -3 and -7, down-regulated the expression of anti-apoptotic proteins of Bcl-x and Bag-1, and upregulated the levels of proapoptotic proteins of Bad, Bak, Bax and Bim in BEL-7402 cells. These results show that Ru1 induce apoptosis in BEL-7402 cells through ROS-mediated mitochondrial dysfunction pathway.

Keywords: Ru (II) polypyridyl complex; cytotoxicity in vitro; ROS; mitochondrial membrane potential; western blot analysis; DNA-binding.

1. Introduction

The successful application of cisplatin and its analogues as anticancer drugs, as

well as their therapeutic drawbacks, has fostered a growing number of studies on diverse classes of metal complexes and their biological effects [1]. Ruthenium complex NAMI-A was used as an antimetastatic drug, and KP1019 was employed as an anticancer, and in particular colon carcinomas [2,3]. Interest was stimulated by phase I clinical trials of the two ruthenium complexes. In recent years, studies on ruthenium complexes as anticancer drugs have been paid extensive attention, and some interesting results have been obtained. Complex $[Ru(bpy)_2(2,9\text{-dimethyl-dpq})]^{2+}$ has no cytotoxicity toward A549 cells in the dark with an IC_{50} values of 250 (± 5) μM, but irradiated with > 450 nm light for 3 min, the complex shows high cytotoxic effect with an IC_{50} value of 1.2 (± 0.1) μM [4]. Complex $[Ru(3,4,7,8\text{-tmp})_2(dmdppz)]^{2+}$ shows high cytotoxicity against non-small lung carcinoma cell line (NCI-H460) (IC_{50} = 7.0 μM) [5]. T*rans*-$[RuCl_3(H_2O)(dbtp)_2]$ and *mer*-$[RuCl_3(dbtp)_3]$ show excellent cytotoxicity with IC_{50} values in the range of 0.02–2.4 μM against A549 and T47D cell lines [6]. Polypyridyl Ru(II) complex $[Ru(dip)_2(1\text{-Py-}\beta C)]^{2+}$ shows high inhibition of cell growth toward HeLa (IC_{50} = 1.9 ± 0.2 μM) [7], and Λ-$[Ru(phen)_2(p\text{-MOPIP})]^{2+}$ exhibits a significant antitumor activity in HepG2 cells [8]. Schatzscneider reported that complex $[Ru(bpy)_2(dppn)]^{2+}$ (dppn = benzo[i]dipyrido[3,2-*a*:2',3'-*c*]phenazine) exhibits a low micromolar IC_{50} value against HT-29 cell line comparable to cisplatin under similar conditions [9]. Ru(II) complex containing dppn ligand with good planarity shows high cytotoxicity in vitro, which prompts us to design a ligand addppn with extended planarity compared with dppn. In our previous studies, we found complexes $[Ru(dmb)_2(addppn)]^{2+}$ and $[Ru(bpy)_2(addppn)]^{2+}$ exhibit very high

cytotoxic effect toward tumor cell lines [10]. Phen as ancillary ligand has good hydrophobicity, as expected, complex $[Ru(phen)_2(addppn)]^{2+}$ should have high cytotoxic activity against selected tumor cell lines. To investigated the effect of $[Ru(phen)_2(addppn)]^{2+}$ on the growth of cancer cells, in this report, complex $[Ru(phen)_2(addppn)](ClO_4)_2$ (Ru1) (addppn = acenaphtheno[1,2-b]-1,4-diazabenzo[i]dipyrido[3,2-*a*:2',3'-*c*]phenazine, phen = 1,10-phenanthroline, Scheme 1) was synthesized and characterized by elemental analysis, ES-MS, ^{1}H NMR and ^{13}C NMR. The cytotoxicity in vitro of Ru1 was assessed by MTT assays (MTT = (3-(4,5-dimethylthiazol-2-yl)-2,5-diphenyltetrazolium bromide)). The apoptosis of BEL-7402 cells induced by Ru1 was studied by fluorescent microscopy and flow cytometry. The reactive oxygen species (ROS) and cell cycle arrest were analyzed by flow cytometry. The change in mitochondrial membrane potential was determined with fluorescent microscope. The apoptotic pathway was also investigated in detail by western blot analysis. In addition, the DNA-binding behaviors were studied by electronic absorption titration, luminescence spectra, viscosity measurements and photocleavage of pBR322 DNA.

2. Experimental

2.1. Materials and methods

All reagents and solvents were purchased commercially and used without further purification unless otherwise noted. Ultrapure MilliQ water was used in all

experiments. DMSO, acenaphthylene and RPMI 1640 were purchased from Sigma. Cell lines of BEL-7402 (Hepatocellular), HeLa (Human cervical cancer cell line), MG-63 (Human osteosarcoma) and SKBR-3 (Human breast cancer) were purchased from the American Type Culture Collection. $RuCl_3 \cdot 3H_2O$ was purchased from the Kunming Institution of Precious Metals. 1,10-phenanthroline was obtained from the Guangzhou Chemical Reagent Factory.

Microanalyses (C, H, and N) were obtained with a Perkin-Elmer 240Q elemental analyzer. Electrospray ionization mass spectra (ES-MS) were recorded on a LCQ system (Finnigan MAT, USA) using methanol as mobile phase. The spray voltage, tube lens offset, capillary voltage and capillary temperature were set at 4.50 KV, 30.00 V, 23.00 V and 200 ^{o}C, respectively, and the quoted *m/z* values are for the major peaks in the isotope distribution. ^{1}H NMR and ^{13}C NMR spectra were recorded on a Varian-500 spectrometer with DMSO [D_6] as solvent and tetramethylsilane (TMS) as an internal standard at 500 MHz at room temperature.

2.2. Synthesis of ligand and complex

1,10-phenanthroline-5,6-dione [11] and ligand dadppz [10,12] were prepared according to the methods in the literature.

Synthesis of $[Ru(phen)_2(addppn)](ClO_4)_2$ (Ru1)

A mixture of $[Ru(phen)_2(dadppz)] \cdot 2H_2O$ [13] (0.486 g, 0.5 mmol) and acenaphthequinone (0.091 g, 0.50 mmol) in dimethylformamide (20 cm^3) was

refluxed under argon for 8 h, then removed solvent under reduced pressure to about 3 cm^3. Upon cooling, a red precipitate was obtained by dropwise addition of saturated aqueous $NaClO_4$ solution. The crude product was purified by column chromatography on neutral alumina with a mixture of CH_3CN-C_2H_5OH (5:1, v/v) as eluent. The red band was collected. The solvent was removed under reduced pressure and a red powder was obtained. Yield: 70%. Anal. Calc for $C_{54}H_{30}N_{10}Cl_2O_8Ru$: C, 57.97; H, 2.70; N, 12.52%. Found: C, 57.84; H, 2.82; N, 12.43%. ES-MS (CH_3CN, m/z): 918.5 $[(M\text{-}2ClO_4\text{-}H)]^+$, 459.5 $[(M\text{-}2ClO_4)]^{2+}$. ^1H NMR (DMSO-d_6): 9.34 (d, 2H, J = 7.5 Hz), 8.87 (dd, 6H, J = 8.5, J = 8.5 Hz), 8.46 (s, 6H), 8.30 (d, 2H, J = 6.5 Hz), 8.20 (d, 2H, J = 5.0 Hz), 8.14 (d, 2H, J = 4.5 Hz), 7.87-7.96 (m, 6H), 7.84 (dd, 2H, J = 5.0, J = 5.0 Hz), 7.70 (t, 2H, J =.5 7 Hz). ^{13}C NMR (DMSO-d_6): 155.25, 154.42, 153.22, 152.84, 150.88, 147.33, 147.21, 140.69, 140.21, 139.29, 137.29, 137.15, 133.26, 130.65, 130.19, 129.73, 128.95, 128.42, 127.77, 126.53, 126.36, 122.31.

Caution: Perchlorate salts of metal compounds with organic ligands are potentially explosive, and only small amounts of the material should be prepared and handled with great care.

2.3. In vitro cytotoxicity assays

Standard 3-(4,5-dimethylthiazole)-2,5-diphenyltetraazolium bromide (MTT) assay procedures were used. Cells were placed in 96-well microassay culture plates (8×10^3 cells per well) and grown overnight at 37 °C in a 5% CO_2 incubator. The tested compounds were then added to the wells to achieve final concentrations ranging from

10^{-6} to 10^{-4} M. Control wells were prepared by addition of culture medium (100 μL). The plates were incubated at 37 °C in a 5% CO_2 incubator for 48 h. Upon completion of the incubation, stock MTT dye solution (20 μL, 5 mg·mL^{-1}) was added to each well. After 4 h, buffer (100 μL) containing *N*,*N*-dimethylformamide (50%) and sodium dodecyl sulfate (20%) was added to solubilize the MTT formazan. The optical density of each well was then measured with a microplate spectrophotometer at a wavelength of 490 nm. The IC_{50} values were calculated by plotting the percentage viability versus concentration on a logarithmic graph and reading off the concentration at which 50% of cells remained viable relative to the control. Each experiment was repeated at least three times to obtain the mean values.

2.4. Apoptosis assay by Hoechst 33258 staining

BEL-7402 cells were seeded onto chamber slides in six-well plates at a density of 2 × 10^5 cells per well and incubated for 24 h. The cells were cultured in RPMI 1640 supplemented with 10% of fetal bovine serum (FBS) and incubated at 37 °C and 5% CO_2. The medium was removed and replaced with medium (final DMSO concentration 0.05% v/v) containing Ru1 (12.5 or 25 μM) for 24 h. The medium was removed and the cells were washed with ice-cold PBS, and fixed with formalin (4%, w/v). Cell nuclei were counterstained with Hoechst 33258 (10 μg/mL in PBS) for 10 min, Then observed and imaged by fluorescence microscope (Nikon, Yokohama, Japan) with excitation at 350 nm and emission at 460 nm.

2.5. Apoptosis assay by flow cytometry

After chemical treatment, 1×10^6 cells were harvested, washed with PBS, fixed with 70% ethanol, and finally maintained at 4 ^oC for at least 12 h. The pellets were stained with a fluorescent probe solution containing 50 μg/mL PI and 1 mg/mL annexin in PBS on ice in dark for 15 min. The fluorescence emission was measured at 530 nm and 575 nm (or equivalent) using 488 nm excitation with a FACS Calibur flow cytometry (Beckman Dickinson & Co., Franklin Lakes, NJ). A minimum of 10 000 cells were analyzed per sample.

2.6. Cellular uptake studies

Cells were placed in 24-well microassay culture plates (4×10^4 cells per well) and grown overnight at 37 ^oC in a 5% CO_2 incubator. Different concentrations of Ru1 were then added to the wells. The plates were incubated at 37 ^oC in a 5% CO_2 incubator for 24 h. Upon completion of the incubation, the wells were washed three times with phosphate buffered saline (PBS). After discarding the culture medium, the cells were visualized by fluorescent microscopy.

2.7. Cell cycle arrest by flow cytometry

BEL-7402 or SKBR-3 cells were seeded into six-well plates (Costar, Corning Corp, New York) at a density of 1×10^6 cells per well and incubated for 24 h. The cells were cultured in RPMI 1640 supplemented with fetal bovine serum (FBS, 10%) and incubated at 37 °C and 5% CO_2. The medium was removed and replaced with

medium (final DMSO concentration 0.05% v/v) containing Ru1 (25 or 50 μM). After incubation for 24 h, the cell layer was trypsinized and washed with cold phosphate buffered saline (PBS) and fixed with 70% ethanol. Twenty μL of RNAse (0.2 mg/mL) and 20 μL of propidium iodide (0.02 mg/mL) were added to the cell suspensions and the mixtures were incubated at 37 °C for 30 min. The samples were then analyzed with a FACSCalibur flow cytometry. The number of cells analyzed for each sample was 10000 [14].

2.8. Reactive oxygen species (ROS) detection

BEL-7402 cells were seeded into six-well plates (Costar, Corning Corp, New York) at a density of 1×10^6 cells per well and incubated for 24 h. The cells were cultured in RPMI 1640 supplemented with 10% of fetal bovine serum (FBS) and incubated at 37 °C and 5% CO_2. The medium was removed and replaced with medium (final DMSO concentration 0.05% v/v) containing Ru1 (12.5 μM) for 24 h. The medium was removed again. The fluorescent dye (CM-H_2DCFDA) was added to the medium with a final concentration of 10 μM to cover the cells. The treated cells were then washed with cold PBS-EDTA twice, collected by trypsinization and centrifugation at 1,500 rpm for 5 min, and resuspended in PBS-EDTA. Fluorescence activated cell sorting flow cytometry was performed to analyze the cells with an excitation wavelength of 488 nm and emission at 525 nm.

2.9. Mitochondrial membrane potential assay

Cells were treated with Ru1 for 24 h in 12-well plates and were then washed three times with cold PBS. The cells were then detached with trypsin-EDTA solution. Collected cells were incubated for 20 min with 1 μg/mL of 5,5',6,6'-tetrachloro-1,1',3,3'-tetraethylbenzimidazolcarbocyanine iodide (JC-1) in culture medium at 37 °C in the dark. Cells were immediately centrifuged to remove the supernatant. Cell pellets were suspended in PBS and then imaged under fluorescence microscope.

2.10. Western blot analysis

BEL-7402 cells were seeded in 3.5-cm dishes for 24 h and incubated with different concentrations of the complex in the presence of 10% FBS. Then cells were harvested in lysis buffer. After sonication, the samples were centrifuged for 20 min at 13,000 g. The protein concentration of the supernatant was determined by BCA assay. Sodium dodecyl sulfate–polyacrylamide gel electrophoresis was done loading equal amount of proteins per lane. Gels were then transferred to poly(vinylidene difluoride) membranes(Millipore) and blocked with 5% non-fat milk in TBST buffer for 1 h. The membranes were incubated with primary antibodies at 1:5,000 dilutions in 5% non-fat milk overnight at 4 °C, and after being washed for four times with TBST for a total of 30 min, then the secondary antibodies conjugated with horseradish peroxidase at 1:5,000 dilution for 1 h at room temperature and washed for four times with TBST. The blots were visualized with the Amersham ECL Plus western blotting detection reagents according to the manufacturer's instructions. To assess the presence of

comparable amount of proteins in each lane, the membranes were stripped finally to detect the β-actin.

Statistical analysis

All of the data were expressed as the mean ± SD. Differences between two groups were analyzed by a two-tailed Student's t test. Differences with $P < 0.05$ were considered statistically significant.

2.11. DNA-binding and photocleavage

The DNA-binding and photoactivated cleavage experiments were performed at room temperature. Buffer A [5 mM tris(hydroxymethyl)aminomethane (Tris) hydrochloride, 50 mM NaCl, pH 7.0] was used for absorption titration, luminescence titration and viscosity measurements. Buffer B (50 mM Tris-HCl, 18 mM NaCl, pH 7.2) was used for DNA photocleavage experiments. Solutions of calf thymus DNA (CT DNA) in buffer A gave a ratio of UV-Vis absorbance of 1.8–1.9:1 at 260 and 280 nm, indicating that the DNA was sufficiently free of protein [15]. The concentration of DNA was determined spectrophotometrically (ε_{260} = 6600 M^{-1} cm^{-1}) [16].

The absorption titrations of the complex in buffer were performed using a fixed concentration (20 μM) for complex to which increments of the DNA stock solution were added. The intrinsic binding constant *K*, based on the absorption titration, was measured by monitoring the changes in absorption at the MLCT band with increasing concentration of DNA using the following equation [17].

$$[DNA]/(\varepsilon_a - \varepsilon_f) = [DNA]/(\varepsilon_b - \varepsilon_f) + 1/[K_b((\varepsilon_b - \varepsilon_f)]$$

where [DNA] is the concentration of DNA in base pairs, ε_a, ε_f and ε_b correspond to the apparent absorption coefficient Aobsd/[Ru], the extinction coefficient for the free ruthenium complex and the extinction coefficient for the ruthenium complex in the fully bound form, respectively. In plots of [DNA]/(ε_a-ε_f) versus [DNA], K_b is given by the ratio of slope to the intercept.

Viscosity measurements were carried out using an Ubbelodhe viscometer maintained at a constant temperature at 25.0 (± 0.1) °C in a thermostatic bath. DNA samples approximately 200 base pairs in average length were prepared by sonication to minimize complexities arising from DNA flexibility [18]. Flow time was measured with a digital stopwatch, and each sample was measured three times, and an average flow time was calculated. Relative viscosities for DNA in the presence and absence of complex were calculated from the relation $\eta = (t - t^0)/t^0$, where t is the observed flow time of the DNA-containing solution and t^0 is the flow time of buffer alone [19, 20]. Data were presented as $(\eta/\eta_0)^{1/3}$ versus binding ratio [21], where η is the viscosity of DNA in the presence of complexes and η_0 is the viscosity of DNA alone.

For the gel electrophoresis experiment, supercoiled pBR 322 DNA (0.1 μg) was treated with the Ru(II) complex in buffer B, and the solution was then irradiated at room temperature with a UV lamp (365 nm, 10 W). The samples were analyzed by electrophoresis for 1.5 h at 80 V on a 0.8% agarose gel in TBE (89 mM Tris-borate acid, 2 mM EDTA, pH = 8.3). The gel was stained with 1 μg/ml ethidium bromide and photographed on an Alpha Innotech IS–5500 fluorescence chemiluminescence

and visible imaging system.

3. Results and discussion

3.1. Cytotoxicity assay in vitro

The in vitro cytotoxicity of the Ru(II) complex was determined against BEL-7402, HeLa, MG-63 and SKBR-3 cell lines using the MTT assay [22]. Given its low aqueous solubility, Ru1 was dissolved in DMSO. And blank samples containing the same amount of DMSO and cisplatin were used as negative and positive controls, respectively. The in vitro cytotoxicity of Ru1 was assessed on selected cell lines based on cell survival after 48 h of exposure to the desired concentration (3.125, 6.25, 12.5, 25 and 50 μM) using the MTT assay. The IC_{50} values are listed in Table 1, and cell viability is depicted in Fig. 1. Comparing the IC_{50} values of Ru1 with cisplatin, the level of cytotoxicity of Ru1 towards BEL-7402 and SKBR-3 cells was unexpectedly found to be higher than that of cisplatin, a classical anti-cancer agent that covalently binds DNA after hydrolysis of its liable ligands. The cytotoxic effect of Ru1 against MG-63 cells is comparable with that of cisplatin under identical conditions. In addition, the in vitro cytotoxicity of Ru1 against selected cell lines is higher than that of $[Ru(bpy)_2(addppn)]^{2+}$ and other Ru(II) complexes reported in our previous work [23-26]. Fig. 1 also shows that the cytotoxic activity of Ru1 is concentration dependent, and the cell viability decreases with increasing Ru1 concentrations.

3.2. Hoechst 33258 staining assay

Most currently used cytotoxic drugs have been found to induce apoptosis in susceptible cells. The fact that disparate agents, that interact with different targets, induce cell death and exhibit some common features (endonucleolytic cleavage of DNA, and changes in chromatin condensation) suggests that cytotoxicity is determined by the capability of the cell in engage this so-called "programmed" cell death [27]. BEL-7402 cells were cultured and exposed to Ru1 (12.5 and 25 μM) for 24 h, and then stained with Hoechst 33258. Apoptotic features such as nuclear shrinkage, and chromatin condensation were observed (Fig. 2). The fluorescent examination of Hoechst 33258-stained BEL-7402 cells revealed that Ru1 induced concentration-dependent apoptosis in the treated cells. These results show that Ru1 can effectively induce apoptosis in BEL-7402 cells.

3.3. Apoptosis assay by flow cytometry

To determine the percentages of apoptosis and necrosis of BEL-7402 cells, the cells were treated with different concentrations of Ru1 for 24 h, followed by cell apoptosis analyses using flow cytometry. The percentages of living, apoptotic and necrotic cells of BEL-7402 are shown in Fig. 3. In the control, the percentages of early apoptotic (A) and late apoptosis and necrotic (N) cells were 0.00% and 0.01%, respectively. After the treatment with Ru1 at 12.5, 25 or 50 μM for 24 h, the percentages of late apoptosis and necrosis increased from 0.01% to 45.97%, and the percentages of early apoptosis of BEL-7402 cells were 5.74%, 6.44% and 9.44%, respectively. The data show that the apoptotic effect is closely related to the concentrations of the complex, given that

more apoptotic cells were observed with the increasing concentration of the complex.

3.4. Cellular uptake studies

The cellular uptake characteristics of a small molecule are critical to its application as a therapeutic or diagnostic agent [28]. Although transition metal complexes have increasingly been employed in biological applications, their uptake properties remain under developed [29-32]. When BEL-7402 cells were exposed to 12.5 or 25 μM of Ru1 for 1, 6, 12 and 24 h, as shown in Fig. 4, bright red fluorescent spots in the images were observed. When BEL-7402 cells were incubated with 12.5 μM of Ru1 for 1 h (b), the fluorescence at the nuclei was not as evident as the other fluorescence images. With increasing Ru1 concentration and prolonged incubation time, more red fluorescent spots were observed. The results show that Ru1 can be successfully uptake by BEL-7402 cells.

3.5. Cell cycle arrest studies

The effect of Ru1 on the cell cycle of BEL-7402 and SKBR-3 cells was investigated using flow cytometry in propidium-iodide-stained cells after Ru(II) complex treatment for 24 h. The representative DNA distribution histograms of BEL-7402 and SKBR-3 cells are shown in Fig. 5a, 5b and 5c. After the treatment of BEL-7402 cells with Ru1, an evident enhancement of 10.42% in the percentage of cells at the G0/G1 phase was observed, accompanied by a corresponding reduction of 6.88% in the percentage of cells in S phase. This observation indicates that the

anti-proliferative mechanism induced by Ru1 on BEL-7402 cells was a G0/G1 phase arrest. While different concentrations of Ru1 were exposed to SKBR-3 cells for 24 h, an enhancement of 8.66% (at 25 μM) and 24.01% (at 50 μM) in the percentage of cells at the G2/M phase was found, which suggests that the anti-proliferative mechanisms induced by Ru1 on SKBR-3 cells are G2/M phase arrest. These results show that Ru1 exhibits different anti-proliferative mechanisms against different cancer cells.

3.6. Measurement of intracellular reactive oxygen species levels

In cancer cells, there is a crucial role of reactive oxygen species (ROS) in cell growth and apoptosis [33]. To investigate whether the cell death induced by Ru(II) complex is dependent on ROS levels, BEL-7402 cells were treated with Ru1 for 24 h, and then ROS levels were evaluated with flow cytometry using 2',7'-dichlorodihydrofluorescein diacetate (DCFH-DA) probe [34,35], this cell-permeant dye is cleaved by intracellular esterases into its non-fluorescent form (DCFH). The non-fluorescent substrate is oxidized by intracellular free radicals to produce a fluorescent product, namely, dichlorofluorescein (DCF). As shown in Fig. 6, ROS generation in BEL-7402 cells treated with Ru1 increased as indicated by the increasing DCF fluorescent intensity. Therefore, Ru1 can enhance the level of intracellular ROS and facilitate the cells apoptosis.

3.7. Mitochondrial membrane potential detection

Mitochondria act as a point of integration for apoptotic signals originating from both extrinsic and intrinsic apoptotic pathways [36,37]. The changes in mitochondrial membrane potential were detected using the fluorescent probe JC-1. JC-1, a lipophilic cationic dye, easily passes through the plasma membrane into cells and accumulates in actively respiring mitochondria [38]. JC-1 forms J-aggregates, which possess a red fluorescence emission peak corresponding to high mitochondrial membrane potential. At low mitochondrial membrane potential, JC-1 forms monomers, which emit a green fluorescence peak. Fig. 7 shows the changes in BEL-7402 cells fluorescence as a result of Ru1 treatment. The control (a, BEL-7402 cells) loaded with JC-1 exhibited a heterogeneous distribution of red fluorescence (JC-1 aggregates) and green fluorescence (JC-1 monomers). After the treatment of BEL-7402 cells with 12.5 μM of Ru1 (b) for 24 h, the red fluorescence decreased whereas the green fluorescence intensity increased in the cytoplasm. The changes from red fluorescence into green fluorescence indicate a decrease in mitochondrial membrane potential.

3.8. Assay of the expression of casapase, antiproteins and proproteins

Caspases are known to mediate the apoptotic pathway [39,40]. Activation of caspase -3, -7, -8, -9 as well as procaspase 7 was assayed by western blot analysis. After the treatment of BEL-7402 cells with different concentrations of Ru1, the levels of caspase -3 and -7 expression increased, whereas that of procaspase 7, caspase -8 and -9 diminished (Fig. 8a). Bcl-2 family proteins play a critical function in apoptotic regulation via the control of mitochondrial membrane permeability. Whether Ru1 can

induce changes in the levels of the Bcl-2 family protein was determined. Fig. 8b shows that the treatment of anti-apoptotic proteins Bcl-2, Bcl-x and Bag-1 with different concentrations Ru1 does not evidently induce changes in the levels of Bcl-2 protein. The expression of Bcl-x and Bag-1 was down-regulated. Treatment of Bad with 50 μM of Ru1, the expression of Bad was downregulated. However, treatment of Bak, Bax and Bim with different concentrations of Ru1, no obvious changes in the levels of proapoptotic protein Bak, Bax and Bim, were observed. These results suggest that Ru1 induces BEL-7402 cells death through the activation of the caspase 3, caspase 7 and ROS-mediated mitochondrial dysfunction pathways.

3.9. Electronic absorption titration

As shown in Fig. 9, the spectra of the complex consist of three well-resolved bands in the range of 200–600 nm. Ru1 displays a strong MLCT band at 400–500 nm attributed to overlap the Ru(dπ)→phen(π*) and Ru(dπ)→addppn (π*). At high energy (300→350 nm), the spectra display a large change band, corresponding to (addppn)→π* and π→π* transitions. The band below 300 nm is attributed to intraligand (IL) transition.

Electronic spectra are the commonest way to investigate the interaction of complex with DNA. A complex bound to DNA through intercalation usually results in hypochromism and red shift (bathochromism) owing to the intercalation mode involving a strong stacking interaction between an aromatic chromophore and the base pairs of DNA. Fig. 9 shows that the hypochromism at the MLCT band (460 nm)

is 20.3% with increasing DNA concentration. The DNA-binding constant is determined by monitoring the absorption change in the MLCT band. The value of the intrinsic binding constant K_b is derived to be 1.93 (± 0.12) × 10^6 M^{-1}. The value is comparable to those of Ru(II) complexes such as $[Ru(bpy)_2(ppd)]^{2+}$ (ppd = pteridino[7,6-*f*][1,10] phenanthroline-1,13-(10*H*,12*H*)-dione, *K*= 1.3 × 10^6 M^{-1}) [41] and $[Ru(bpy)_2(dppz)]^{2+}$ (4.9 × 10^6 M^{-1}, dppz = dipyrido[2,3-*a*:3',2'-*c*]phenazine) [42], but less than that of $[Ru(phen)_2(HBT)]^{2+}$ (4.65 × 107 M-1, HBT = 11H,13H-4, 5,9,10,12,14-hexaaza-benzo[*b*]triphenylene) [43].

3.10. Luminescence spectra studies

Emission intensity of Ru1 from the MLCT excited states upon excitation at 460 nm is found to depend on DNA concentration. As shown in Fig. 10, upon the addition of DNA, the emission intensities grow to 13.93 times larger than the original. The enhancement of emission intensity is indicative of binding of the complex to the hydrophobic pocket of DNA and be protected by DNA efficiently.

3.11. Viscosity measurements

Hydrodynamic measurements (i.e., viscosity and sedimentation), being sensitive to length changes, are regarded as the least ambiguous and most critical tests for a classic intercalation model in solution in the absence of crystallographic structural data [19,20]. It is well known that a classical intercalation of a ligand into DNA is known to cause a significant increase in the viscosity of a DNA solution due to an

increase in the separation of the base pairs at the intercalative site and, hence, an increase in the overall DNA molecular length [20]. The changes in the viscosity of CT DNA solution induced by Ru1 and ethidium bromide (EB) are shown in Fig. 11. For EB, the proven classic intercalator will exert the maximum effect on the viscosity of DNA. On increasing the amount of Ru1, the relative viscosity of DNA increases steadily. The extent of the increase in viscosity follows the order EB > Ru1. These results show that Ru1 interacts with DNA through intercalative mode.

3.12. Photocleavage of pBR322 DNA by Ru1

Ru1 shows high anticancer activity, and can effectively inhibit the cell growth of selected cell lines. This prompts us to consider whether Ru1 can cleave DNA. Upon irradiation, most of ruthenium(II) polypyridyl complexes can produce singlet oxygen ($^1O_2$ or $O_2^{\bullet}$), which can cleave DNA [23,44-46]. The potential of the present complex to cleave DNA was investigated by gel electrophoresis using plasmid pBR322 DNA. When circular plasmid DNA is subject to electrophoresis, relatively fast migration will be observed for the intact supercoiled form (Form I); If scission occurs on one strand (nicked), the supercoiled will relax to generate a slower-moving open circular form (Form II) [47]. As shown in Fig. 12, No obvious DNA cleavage was observed for controls in which complex was absent, or incubation of the plasmid DNA with the Ru(II) complex in the dark. With increasing concentration of the Ru(II) complexes, the amount of Form I of pBR322 DNA diminishes gradually, while that of Form II increases. These results indicate that scission occurs on one strand (nicked).

Furthermore, the cleavage effect was found to be concentration dependent.

4. Conclusions

A new ruthenium(II) polypyridyl complex $[Ru(phen)_2(addppn)](ClO_4)_2$ (Ru1) was synthesized and characterized. Cytotoxicity in vitro shows that Ru1 shows higher cytotoxicity than cisplatin on BEL-7402 under identical conditions. Hoechst 33258 staining demonstrates that this complex can effectively induce apoptosis of BEL-7402 cells. Apoptotic assay by flow cytometry exhibits the number of apoptotic cells increases with increasing amount of complex. The cell cycle arrest studies show that the anti-proliferative mechanism induced by Ru1 on BEL-7402 and SKBR-3 cells was G0/G1 and G2/M phase, respectively. Ru1 enhances the level of intracellular ROS and induces the decrease of mitochondrial membrane potential. Western blot analysis shows that Ru1 activates caspase -3, and -7, down-regulates the levels of anti-apoptotic proteins of Bcl-x and Bag-1. However, no obvious changes in the expression levels of proapoptotic protein Bak, Bax and Bim, were observed. These results indicate Ru1 induces apoptosis in BEL-7402 cells through the ROS-mediated mitochondrial dysfunction pathways. In addition, Ru1 can effectively cleave pBR322 DNA upon irradiation. The complex interacts with DNA through intercalative mode.

Acknowledgements

This work was supported by the National Nature Science Foundation of China (No 31070858) and Guangdong Pharmaceutical University for financial supports.

Notes and References

1. L. Salassa, *Eur. J. Inorg. Chem*., 2011, 32, 4931-4947.
2. G. Sava, R. Gagliardi, A. Bergamo, E. Alessio, G. Mestroni, *Anticancer Res*., 1999, 19, 969-972.
3. M. Galanski, V. B. Arion, A. M. Jakupec, B. K. Keppler, *Curr. Pharm. Des*., 2003, 9, 2078-2089.
4. B. S. Howerton, D. K. Heidary, E. C. Glazer, *J. Am. Chem. Soc*., 2012, 134, 8324-8327.
5. V. Rajendiran, M. Palaniandavar, V. S. Periasamy, M. A. Akbarsha, *J. Inorg. Biochem*., 2012, 116, 151-162.
6. I. Łakomska, M. Fandzloch, T. Muzioł, T. Lis, J. Jezierska, *Dalton Trans*., 2013, 42, 6219-6226.
7. C. P. Tan, S. S. Lai, S. H. Wu, S. Hu, L. J. Zhou, Y. Chen, M. X. Wang, Y. P. Zhu, W. Lian, W. L. Peng, L. N. Ji, A. L. Xu, *J. Med. Chem*., 2010, 53, 7613-7624.
8. D. D. Sun, Y. N. Liu, D. Liu, R. Zhang, X. C. Yang, J. Liu, *Chem. Eur. J*., 2012, 18, 4285-4295.
9. U. Schatzschneider, J. Niesel, I. Ott, R. Gust, H. Alborzinia, S. Wölfl, *ChemMedChem*, 2008, 3, 1104-1109.
10. Y. Y. Xie, H. L. Huang, J. H. Yao, G. J. Lin, G. B. Jiang, Y. J. Liu, *Eur. J. Med. Chem*., 2013, 63, 603-610.
11. W. Paw, **R.** Eisenberg, *Inorg. Chem*., 1997, 36, 2287-2293.

12. K. Wärnmark, J. A. Thomas, O. Heyke, J. M. Lehn, *Chem. Commun*., 1996, 6, 701-702.

13. Y. Y. Xie, G. J. Lin, G. B. Jiang, Z. H. Liang, H. L. Huang, Y. J. Liu, *Transition Met. Chem*., 2013, 38, 563-571.

14. K. K. Lo, T. K. Lee, J. S. Lau, W. L. Poon, S. H. Cheng, *Inorg. Chem*., 2008, 47, 200-208.

15. J. Marmur, J. Mol. Biol., 1961, 3, 208-218.

16. M. E. Reichmann, S. A. Rice, C. A. Thomas, P. Doty, *J. Am. Chem. Soc*., 1954, 76, 3047-3053.

17. A. Wolf, G. H. Shimer Jr, T. Meehan, *Biochemistry*, 1978, 26, 6392-6396.

18. J. B. Chaires, N. Dattagupta, D. M. Crothers, *Biochemistry*, 1982, 21, 3933-3940.

19. S. Satyanarayana, J. C. Dabrowiak, J. B. Chaires, *Biochemistry*, 1993, 32, 2573-2584.

20. S. Satyanaryana, J. C. Dabrowial, J. B. Chaires, *Biochemistry*, 1992, 31, 9319-9324.

21. G. Cohen, H. Eisenberg, *Biopolymers*, 1969, 8, 45-55.

22. T. Mosmann, *J. Immunol. Methods*., 1983, 65, 55-63.

23. Y. J. Liu, C. H. Zeng, H. L. Huang, L. X. He, F. H. Wu, *Eur. J. Med. Chem*., 2010, 45, 564-571.

24. H. L. Huang, Z. Z. Li, Z. H. Liang, Y. J. Liu, *Eur. J. Inorg. Chem*., 2011, 36, 5538-5547.

25. Y. J. Liu, C. H. Zeng, Z. H. Liang, J. H. Yao, H. L. Huang, Z. Z. Li, F. H. Wu, *Eur.*

J. Med. Chem., 2010, 45, 3087-3095.

26. H. L. Huang, Z. Z. Li, Z. H. Liang, J. H. Yao, Y. J. Liu, *Eur. J. Med. Chem*., 2011, 46, 3282-3290.

27. J. A. Hickman, *Cancer Metast Rev*., 1992, 11, 121-139.

28. C. A. Puckett, J. K. Barton, *J. Am. Soc. Chem*., 2007, 129, 46-47.

29. C. X. Zhang, S. J. Lippard, *Curr. Opin. Chem. Biol*., 2003, 7, 481-489.

30. L. J. K. Boerner, J. M. Zaleski, *Curr. Opin. Chem. Biol*., 2005, 9, 135-144.

31. J. Brunner, J. K. Barton, *Biochemistry*, 2006, 45, 12295-12302.

32. J. R. Hart, O. Glebov, R. J. Ernst, I. L. Kirsch, J. K. Barton, Proc. Natl. Acad. Sci. USA., 2006, 103, 15359-15363.

33. M. E. Juan, U. Wenzel, H. Daniel, J. M. Planas, *J. Agric. Food. Chem*., 2008, 56, 4813-4818.

34. C. P. LaBel, H. Ischiropoulos, S. C. Bondy, *Chem. Res. Toxicol*., 1992, 5, 227-231.

35. J. Ye, S. Wang, S. S. Leonard, Y. Sun, L. Butterworth, J. Antonini, M. Ding, Y. Rojanasakul, V. Vallyathan, V. Castronova, X. Shi, J. Biol. *Inorg. Chem*., 1999, 274, 34974-34980.

36. T. F. Chen, Y. S. Wong, *Int. J. Biochem. Cell. Biol*., 2009, 41, 666-676.

37. T. F. Chen, Y. S. Wong, *Cell. Mol. Life. Sci*., 2008, 65, 2763-2775.

38. A. Malugin, P. Kopečková, J. Kopeček, *Mol. Pharmaceut*., 2005, 3, 351-361.

39. G. S. Salvesen, V. M. Dixit, *Cell*, 1997, 91, 443-446.

40. N. A. Thornberry, Y. Lazebnik, *Science*, 1998, 281, 1312-1316.

41. F. Gao, H. Chao, F. Zhou, Y. X. Yuan, B. Peng, L. N. Ji, *J. Inorg. Biochem*., 2006,

100, 1487-1492.

42. A. E. Friedman, J. C. Chambron, J. P. Sauvage, N. J. Turro, J. K. Barton, *J. Am. Chem. Soc*., 1990, 112, 4960-4962.

43. D. L. Arockiasamy, S. Radhika, R. Parthasarathi, B. U. Nair, *Eur. J. Med. Chem*., 2009, 44, 2044-2051.

44. Y. J. Liu, C.H. Zeng, J.H. Yao, F.H. Wu, L.X. He, H.L. Huang, *Chem & Biodivers*., 2010, 7, 1770-1783.

45. F. Gao, H. Chao, F. Zhou, Y.X. Yuan, B. Peng, L. N. Ji, *J. Inorg. Biochem.*, 2006, 100, 1487-1494.

46. L. F. Tan, X. L. Liang, X. H. Liu, *J. Inorg. Biochem.*, 2009, 103, 441-447.

47. J. K. Barton, A. L. Raphael, *J. Am. Soc. Chem*., 1984, 106, 2466-2468.

Captions for Schemes and Figures:

Scheme 1 The structure of Ru1

Fig. 1 Cell viability of **Ru1** on BEL-7402, HeLa, MG-63 and SKBR-3 cells proliferation in vitro. Each point is the mean ± standard error obtained from three independent experiments.

Fig. 2 Hoechst 33258 staining of BEL-7402 cells for 24 h. a) control, b and c treated with 12.5 and 25 μM of **Ru1**, respectively.

Fig. 3 Percentages of Living (L), Necrotic (N) and Apoptotic (A) cells after BEL-7402 (a) exposed ro 12.5 μM (b), 25 μM (c), 50 μM (d) of Ru1 for 24 h analyzed by FACS calibur flow cytometry.

Fig. 4 Bright field, fluorescence and overlay microscopy images of BEL-7402 cells incubated with 12.5 or 25 μM of **Ru1** at 37 ^{o}C for 1, 6, 12 and 24 h.

Fig. 5 Cell cycle distribution of BEL-7402 (a) exposure to **Ru1** 6.25 μM (b), 25 μM (c) and SKBR-3 (d) exposure to **Ru1** 25 μM (e) and 50 μM (f) for 24 h.

Fig. 6 The effect of Ru1 on reactive oxygen species (ROS) generation in BEL-7402 cells exposed to 12.5 μM of Ru1 for 24 h. The significance of the differences between the mean values was determined by using a student's t test. Results were considered significant at $p < 0.05$, which are marked by *.

Fig. 7 Assay of BEL-7402 cells mitochondrial membrane potential with JC-1 as fluorescence probe staining method. a) Control, b) exposed to 12.5 μM of **Ru1** for 24 h.

Fig. 8 Western blot analysis of caspase-3, -7, -8, -9, procaspase 7 (a), Bcl-2, Bcl-x, Bag-1, Bak, Bax and Bim (b) in BEL-7402 cells treated with different concentrations of **Ru1**. β-actin was used as internal control.

Fig. 9 Absorption spectra of Ru1 in Tris-HCl buffer upon addition of CT DNA. [Ru] = 20 μM. Arrow shows the absorbance change upon the increase of DNA concentration. Plots of [DNA] / (ε_a-ε_f) versus [DNA] for the titration of DNA with Ru(II) complex.

Fig. 10 Emission spectra of Ru1 in Tris-HCl buffer in the absence and presence of CT DNA. Arrow shows the intensity change upon increasing DNA concentrations.

Fig. 11 Effect of increasing amounts of complex Ru1 on the relative viscosity of CT DNA at 25 (± 0.1) ^{o}C. [DNA] = 250 μM.

Fig. 12 Photoactivated cleavage of pBR322 DNA in the presence of different concentrations of Ru1 upon irradiation at 365 nm for 30 min.

Table 1 IC_{50} values of **Ru1** toward the selected cell lines.

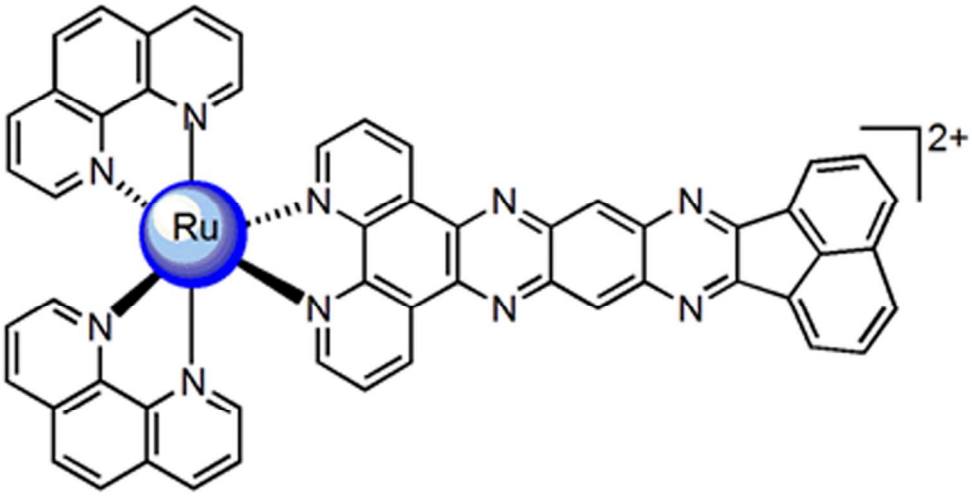

Scheme 1 The structure of Ru1

96x60mm (300 x 300 DPI)

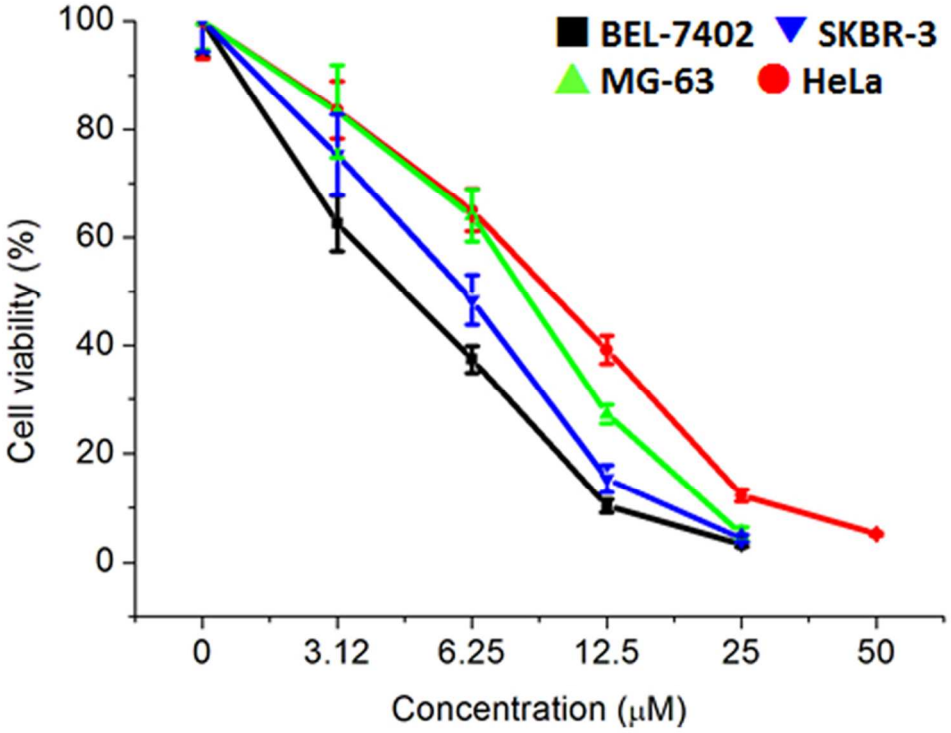

Fig.1 Cell viability of Ru1 on BEL-7402, HeLa, MG-63 and SKBR-3 cells proliferation in vitro. Each point is the mean ± standard error obtained from three independent experiments.

67x60mm (300 x 300 DPI)

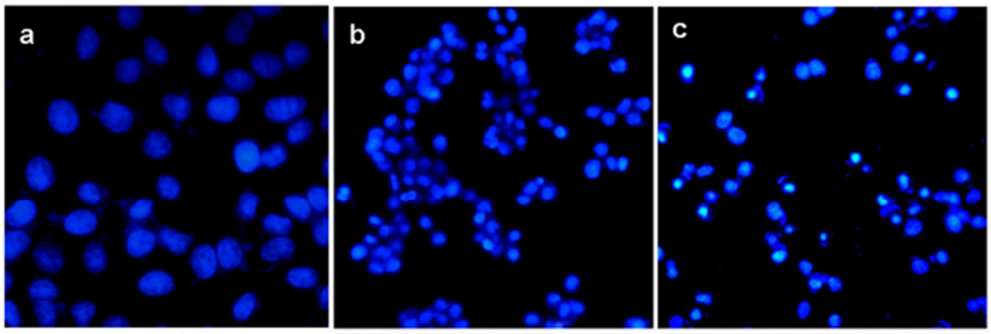

Fig. 2 Hoechst 33258 staining of BEL-7402 cells for 24 h. a) control, b and c treated with 12.5 and 25 μM of complex Ru1, respectively.

54x22mm (300 x 300 DPI)

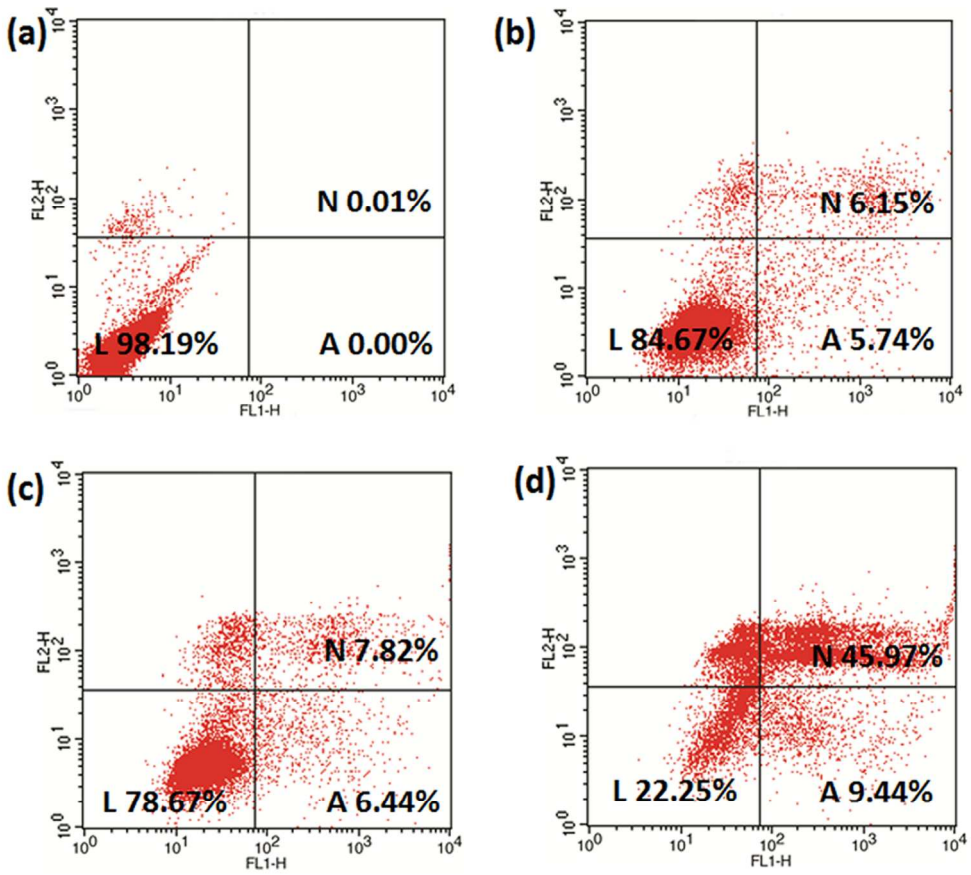

Fig. 3 Percentages of Living, Necrotic and Apoptotic cells after BEL-7402 (a) exposed ro 12.5 µM (b), 25 µM (c), 50 µM (d) of Ru1 for 24 h analyzed by FACS calibur flow cytometry.

201x199mm (300 x 300 DPI)

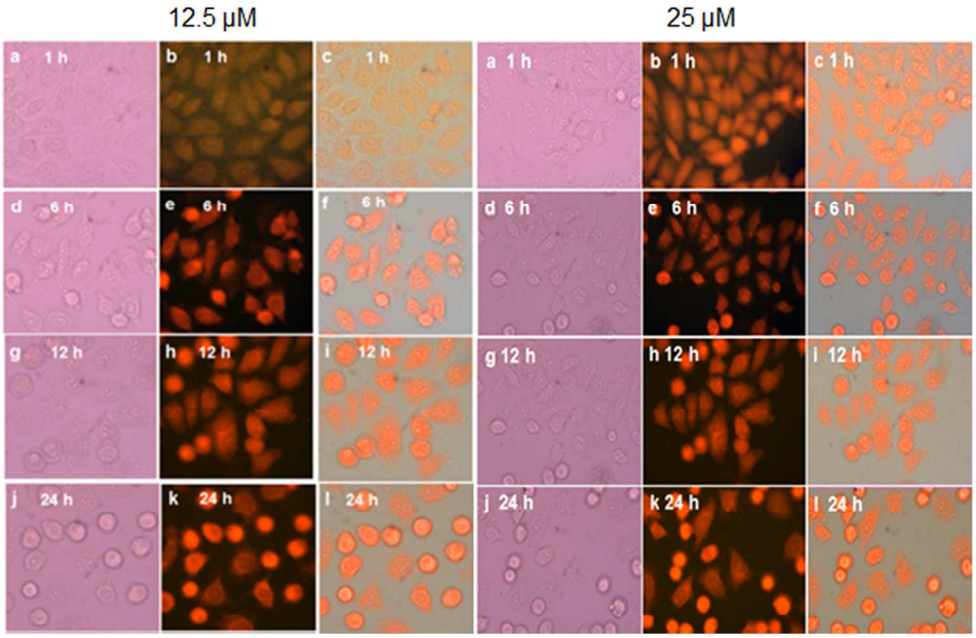

Fig. 4 Bright field (a, d, g, j), fluorescence (b, e, h, k) and overlay (c, f, i, l) microscopy images of BEL-7402 cells incubated with 12.5 and 25 μM Ru1 at 37 °C for 1, 6, 12 and 24 h.

167x119mm (300 x 300 DPI)

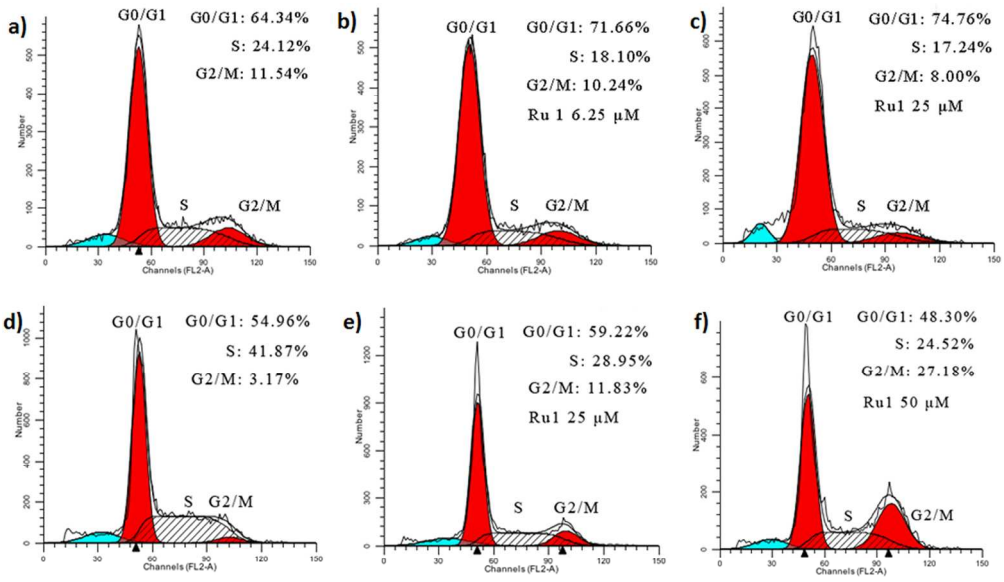

Fig. 5 Cell cycle distribution of BEL-7402 (a) exposure to Ru1 6.25 μM (b), 25 μM (c) and SKBR-3 (d) exposure to Ru1 25 μM (e) and 50 μM (f) for 24 h.

308x199mm (300 x 300 DPI)

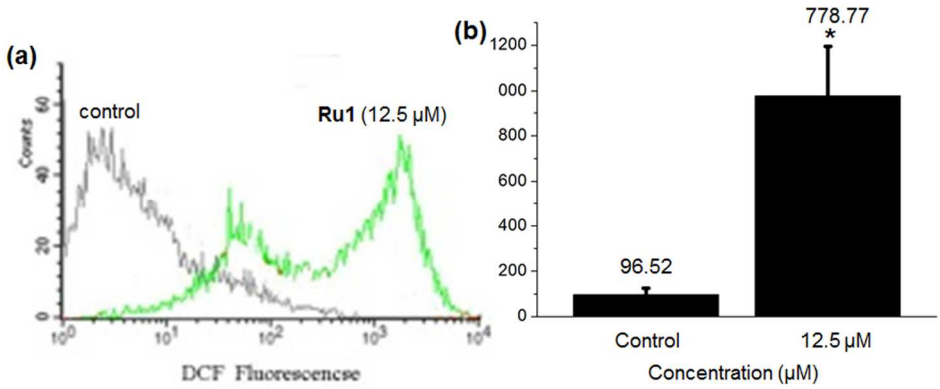

Fig. 6 The effect of Ru1 on reactive oxygen species (ROS) generation in BEL-7402 cells exposed to 12.5 μM of Ru1 for 24 h. The significance of the differences between the mean values was determined by using a student's *t* test. Results were considered significant at $p < 0.05$, which are marked by*.

137x70mm (300 x 300 DPI)

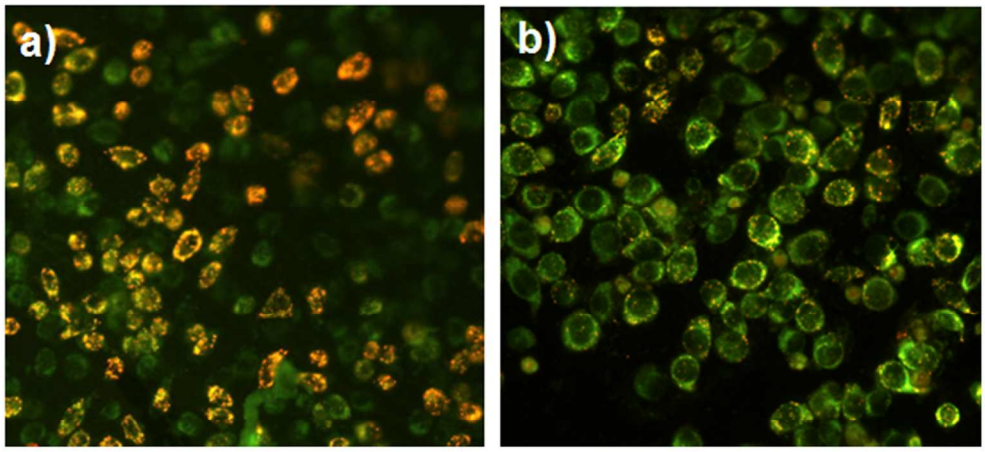

Fig. 7 Assay of BEL-7402 cells mitochondrial membrane potential with JC-1 as fluorescence probe staining method. a) control, b) exposed to 12.5 μM of Ru1 for 24 h.

100x53mm (300 x 300 DPI)

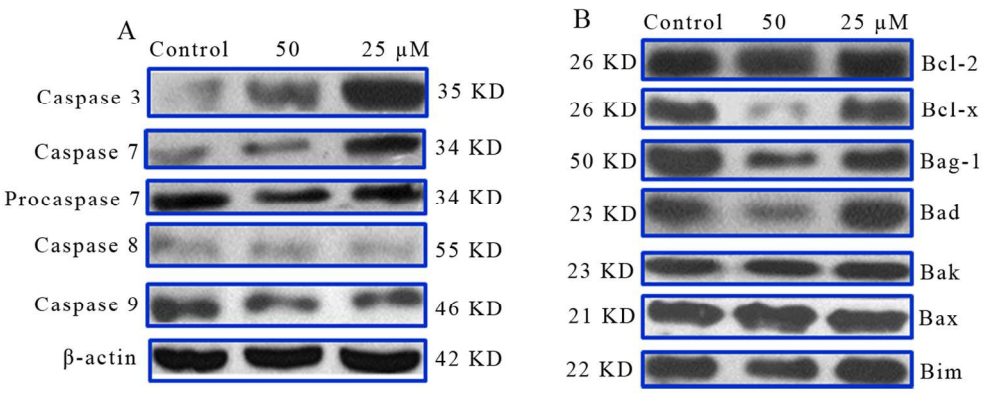

Fig. 8 Western blotting analysis of caspase-3, -7, -8, -9 and procaspase-7 (A),bcl-2, bcl-x, bag-1, bad, bak, bax and bim (B) in BEL-7402 cells treated with different concentrations of Ru1. β-actin was used as internal control.

119x60mm (300 x 300 DPI)

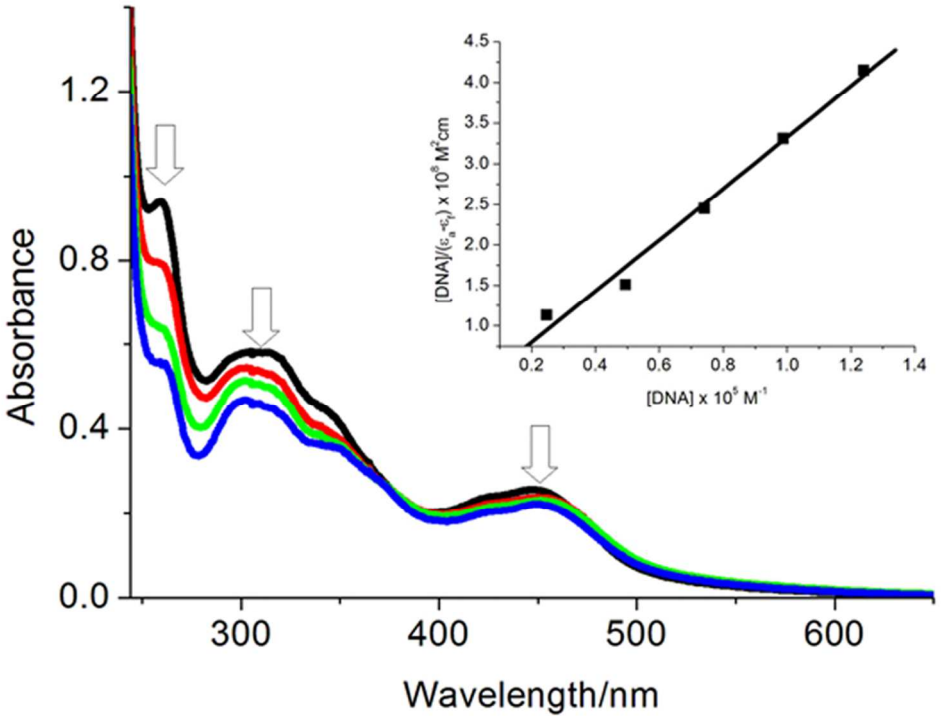

Fig. 9 Absorption spectra of Ru1 in Tris-HCl buffer upon addition of CT DNA. [Ru] = 20 μM. Arrow shows the absorbance change upon the increase of DNA concentration. Plots of [DNA] / (ε_a-ε_f) versus [DNA] for the titration of DNA with Ru(II) complex

85x80mm (300 x 300 DPI)

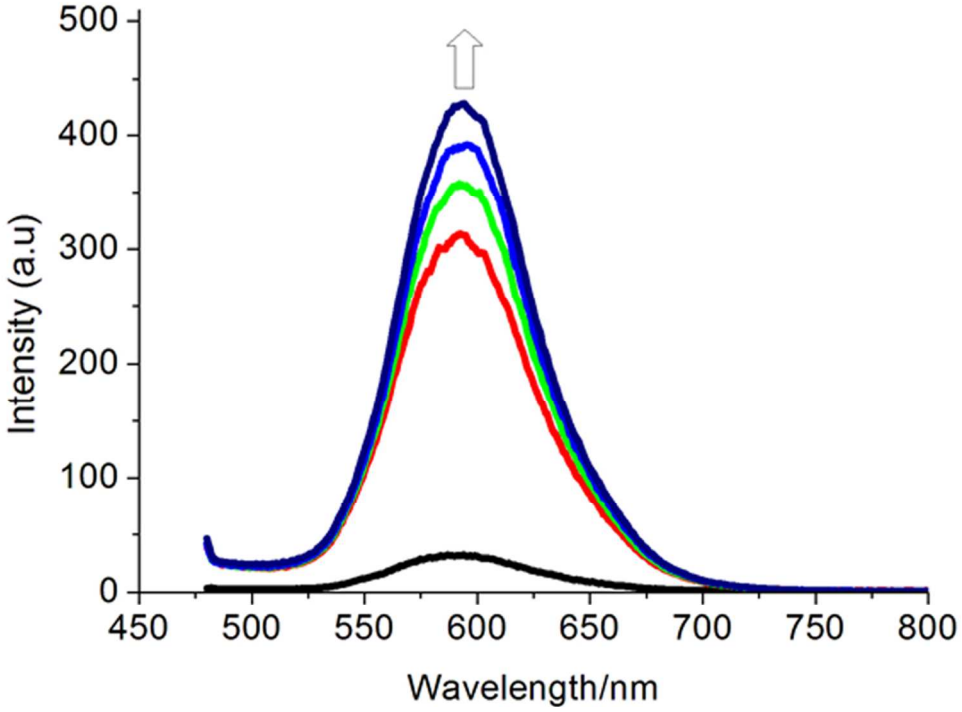

Fig. 10 Emission spectra of Ru1 in Tris-HCl buffer in the absence and presence of CT DNA. Arrow shows the intensity change upon increasing DNA concentrations.

87x80mm (300 x 300 DPI)

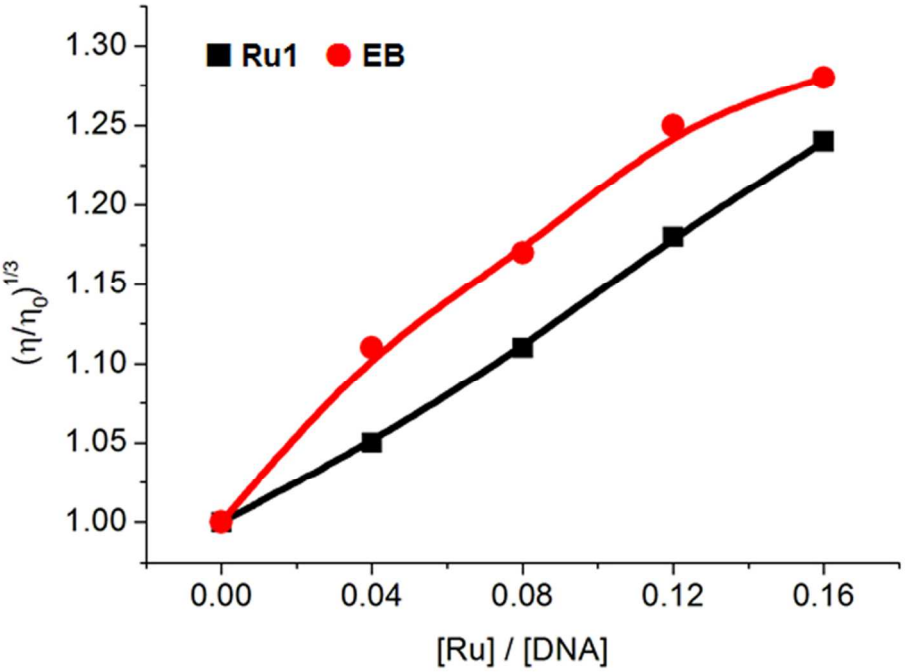

Fig. 11 Effect of increasing amounts of complex Ru1 and EB on the relative viscosity of CT DNA at 25 (± 0.1) ℃. [DNA] = 250 μM.

89x70mm (300 x 300 DPI)

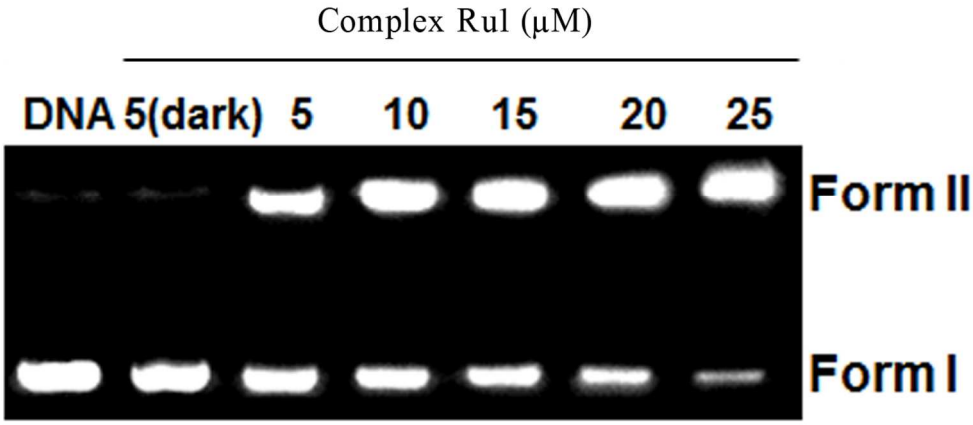

Fig. 12 Photoactivated cleavage of pBR322 DNA in the presence of different concentration of Ru1 upon irradiation at 365 nm for 30 min.

114x70mm (300 x 300 DPI)

Table 1 IC_{50} values of **Ru1** toward the selected cell lines.

Complex	IC_{50} (μM)			
	BEL-7402	HeLa	MG-63	SKBR-3
Ru1	3.9 ± 0.4	9.0 ± 0.8	6.6 ± 0.6	5.1 ± 0.6
cisplatin	13.7 ± 1.8	7.3 ± 1.4	6.5 ± 0.5	6.8 ± 0.5